ELSEVIER

Journal of Alloys and Compounds 262–263 (1997) 502–507

Journal of ALLOYS AND COMPOUNDS

Field- and anisotropy-induced states in $MnAs_{1-x}P_x$-single crystals

Ch. Kleeberg[a,*], A. Vetcher[b], H. Dunkel[a], J.W. Schünemann[c], K. Bärner[a]

[a] *4. Phys. Institut der Univ. Göttingen, Bunsenstr. 11–15, D-37073 Göttingen, Germany*
[b] *Institute of Physics of Solids and Semiconductors, P. Brovki 17, 220072 Minsk, Belarus*
[c] *Lorenz Meßgerätebau, Bundesstr. 116, D-37191 Katlenburg-Lindau, Germany*

Abstract

Field-induced transitions have been observed earlier in manganese monopnictide polycrystals. However, the role played by anisotropy in these second order transitions remained unclear. In this contribution we present magnetization data for 4.2 K $< T <$ 350 K and $0 < B <$ 0.58 T, which demonstrate the field- and anisotropy-determined states of $MnAs_{0.83}P_{0.17}$ and $MnAs_{0.88}P_{0.12}$ single crystals and a clamped state of $MnAs_{0.97}P_{0.03}$. An attempt is made to describe these new combined anisotropy- and field-related states. © 1997 Elsevier Science S.A.

Keywords: Magnetic phase transitions (75.30 K); Magnetic anisotropy (75.30 G); Metastable phases (64.60 M); Electrical conductivity of transition metal compounds (72.80 G)

1. Introduction

Unusual stable and metastable magnetic states and transitions between them have been observed in $MnAs_{1-x}P_x$ polycrystals [1–7]. However, the influence of magnetocrystalline anisotropy on these transitions can only be detected when one uses single crystals. In this contribution, we describe some of these field- and anisotropy-related states. In particular, we present magnetization and resistivity data which demonstrate a clamped state of $MnAs_{0.97}P_{0.03}$, field-induced and combined field- and anisotropy-induced states of $MnAs_{0.83}P_{0.17}$ and of $MnAs_{0.88}P_{0.12}$ single crystals.

2. Experimental and results

Single crystals of $MnAs_{1-x}P_x$ were grown using the Bridgeman–Stockbarger method as described in detail elsewhere [3]. Resistivity and magnetisation were measured using the standard four-probe technique and the Faraday method, respectively. For anisotropic magnetisation measurements sample disks were usually cut in such a way that the disk plane was parallel to the (010) planes and contained both the [010] and [001] direction (orthorhombic notation, $a < c < b$; $c_{hex} \| c$). Occasionally cuts parallel to the (100) and (001) planes were used.

2.1. Clamped states of $MnAs_{0.97}P_{0.03}$

$MnAs_{0.97}P_{0.03}$ is a hexagonal ferromagnet (state I) whose free energy is very close to that of the orthorhombic helical state (II') of, e.g. $MnAs_{0.96}P_{0.04}$. Both states transform into each other in a first-order transition and therefore metastable regions, ΔT, Δx are expected to exist. As hydrostatic pressure is almost equivalent to x it can also shift state I into state II' under a pressure hysteresis Δp. However, in case of Δx, internal strain could clamp state II' in a

* Corresponding author.

0925-8388/97/$17.00
PII S0925-8388(97)00363-0

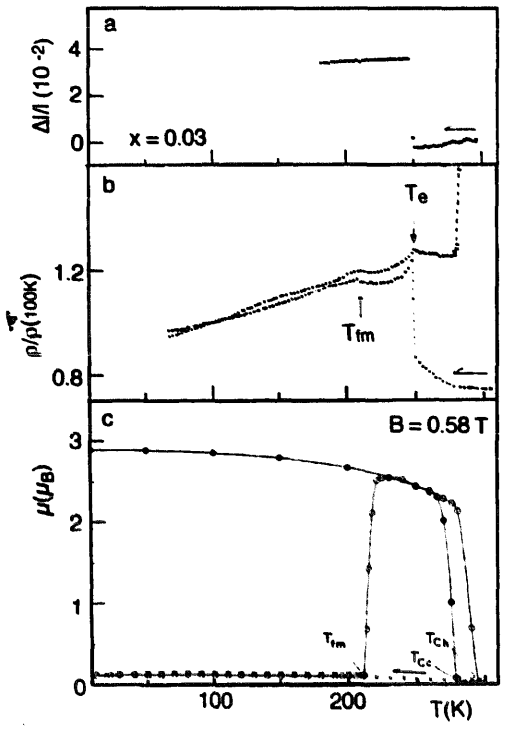

Fig. 1. Irreversible and reversible changes of magnetic moment (c), resistivity in the (100)-direction (b) and step in relative dilatation (a) of single crystal sample $MnAs_{0.97}P_{0.03}$ on the first and second cooling–heating cycle: T_{fm}, irreversible step in magnetic moment; T_e, irreversible step in relative dilatation; $T_{ch} - T_{cc}$, hysteresis connected with the first-order *fm–sg* transition.

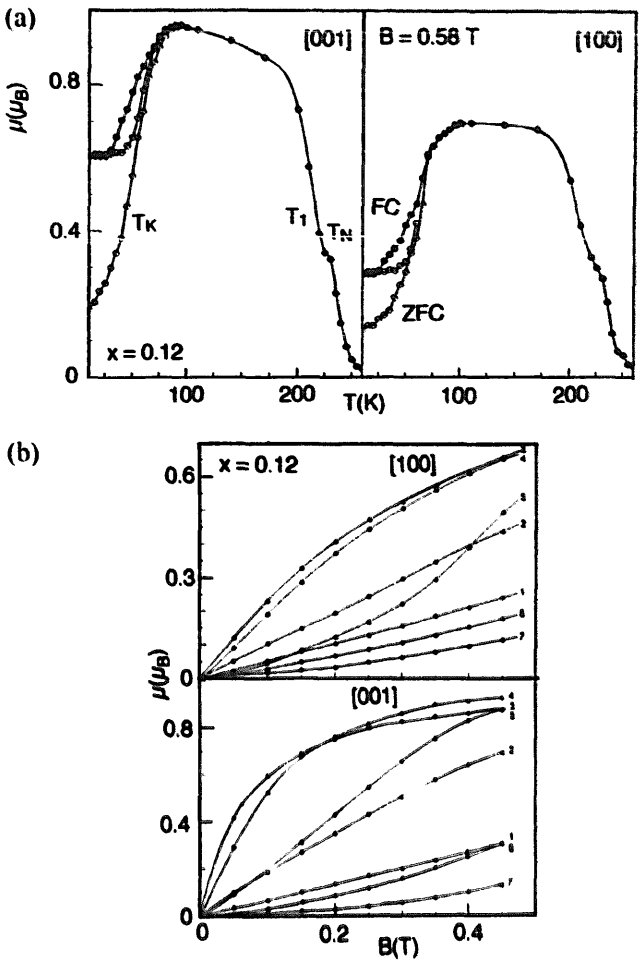

Fig. 2. Magnetic moment vs. temperature (a) and field (b) for a $MnAs_{0.88}P_{0.12}$ single crystal in two crystal directions, B in (010) plane. 1–7: 220 K, 200 K, 150 K, 100 K, 70 K, 40 K, 10 K; fc, field cooled; zfc, zero field cooled; T_K,T_1, magnetic order–order transition temperatures; T_N, *afm*-spin glass like state transition temperature.

metastable situation which will change (irreversibly) into state I only under release of that strain. Shown in Fig. 1 is the first cooling and heating cycle of the resistivity $\rho(T)$ (b) and the magnetization $M(T)$ (c) of a $MnAs_{0.97}P_{0.03}$ single crystal. On heating, $M(T)$ shows a one-time transition from a spin compensated to a ferromagnetic state at a temperature T_{fm}; further heating and cooling cycles only show a hysteretic ($T_{ch} - T_{cc}$) first order transition like that observed in MnAs [4,5], suggesting that the internal strains are released. More details are shown in the resistivity vs. temperature curve $\rho(T)$ (Fig. 1b): the first cooling displays a transition at $T_e \approx 250$ K which could well signal the introduction of long-range helical order in a metastable situation, considering that T_e is very close to the ordering temperature T_N of the stable helical state II′ [7]. The transition at T_e is further established by a pronounced step in the relative dilatation of the sample[1] [8,9] (Fig. 1a).

2.2. Temperature-induced order–order transitions in single crystals

Fig. 2a shows the magnetization of $MnAs_{0.88}P_{0.12}$. This compound shows a sequence of ordered magnetic states with increasing temperature and at higher temperatures finally goes over into the paramagnetic state; in particular, the sequence: helical (0 K < T < 50 K)–canted or conical (50 K < T < 200 K)–helical (200 K < T < 225 K)–spin-glass-like (250 K < T < 350 K) –paramagnetic (T > 350 K) has been proposed [7,10]. Among those, the helical state is rather easily (B ≤ 0.5 T) transformed into canted states as can be seen from the $M(B)$-curves (Fig. 2b). Two different low temperature states are obtained depending on whether the sample is cooled under a magnetic field (FC) or cooled in zero field (ZFC). This is a standard procedure used with disordered magnetic systems. Here, the low magnetisation state (ZFC) is not disordered but long-range ordered (helix) [7]. This suggests that the field-induced high magnetisation state (FC) is also ordered.

The magnetic moment of $MnAs_{0.83}P_{0.17}$ vs. temperature is shown in Fig. 3a; basically, $M(T)$ is very

[1] Courtesy R. Burckart, III, Phys. Institut, University of Göttingen, Bürgerstr. 42–44, D-37073 Göttingen.

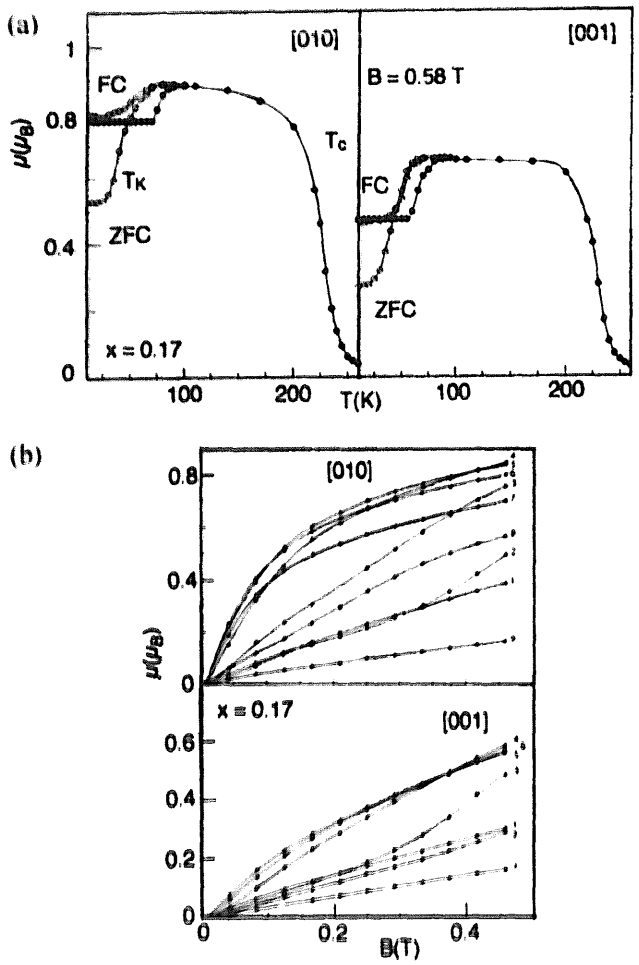

Fig. 3. Magnetic moment vs. temperature (a) and field (b) for a $MnAs_{0.83}P_{0.17}$ single crystal in two crystal directions, B in the (100) plane.
1–9: 10 K, 30 K, 50 K, 70 K, 100 K, 150 K, 200 K, 220 K, 240 K; T_c, canted-sg transition temperature.

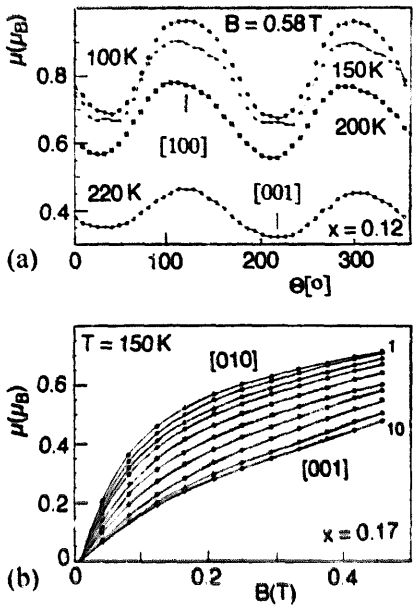

Fig. 4. Anisotropy of the magnetic moment at $B = 0.58$ T and different temperatures for a $MnAs_{0.88}P_{0.12}$ single crystal (a) and anisotropy of $MnAs_{0.83}P_{0.17}$ (b) at $T = 150$ K and different fields. 1–10: [010], 10, 20, 30, 40, 50, 60, 70, 80°C [001].

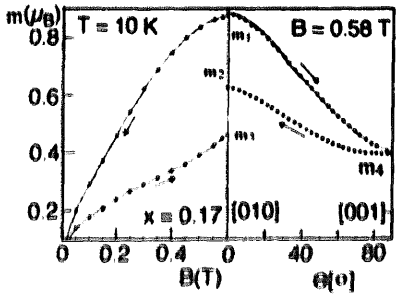

Fig. 5. Hysteresis of magnetization for $MnAs_{0.83}P_{0.17}$ at 10 K obtained using field-sweeps (left side) and an orientational sweeps (right side). m_1, m_2, m_3: stable or metastable states of $MnAs_{0.83}P_{0.17}$ at $B = 0.58$ T in the (010) direction and 10 K.

similar to that of $x = 0.12$, except that the helical state around 250 K has almost vanished ($T_1, T_N \rightarrow T_c$). The $M(B)$-curves (Fig. 3b) are also very similar and suggest field-induced transitions close to the order–order transition temperatures.

2.3. *Anisotropy and field-induced magnetic states*

An anisotropy of the magnetization is observed for both compounds, $x = 0.12$, $x = 0.17$ (Figs. 2–4) and the differences between easy and hard magnetization are comparable in magnitude with the field-induced changes in magnetization which apparently sets the stage for an unusual behaviour of the magnetization when the sample is rotated under a constant field (Fig. 5). With a magnetic state in thermodynamic equilibrium, one would expect to obtain the same magnetization, given the magnetic field B, the temperature T and the orientation θ, independent of the order of installation of these parameters. With a hysteresis existing, as indicated by the field sweep under fixed orientation (left hand side of Fig. 5), one could have one stable and another metastable state, i.e. two relative minima of the free energy, one, for example representing a canted state, the other a helical state. Apparently, this is not sufficient for $MnAs_{0.83}P_{0.17}$ at $T = 10$ K (Fig. 5). If one starts at the highest magnetization m_1, field and temperature being constant, and turns the sample into the hard direction (right hand part of Fig. 5), the magnetization drops to a lower 'hard' value: m_4; turning the sample back under constant H, T, without a hysteresis, one would expect to recover m_1. Considering a hysteresis, one would expect to find the lower (helical) state, m_3. However, the sample stays in a third metastable state, m_2. In the discussion, we will have to consider the origin of the extra metastable state, m_2.

3. Discussion

3.1. Field-induced transitions

$MnAs_{1-x}P_x$ crystals have been considered to be double exchange/super-exchange systems [11,12]. Double exchange and super-exchange in comparable strength and in competition indeed show field-induced transitions; in order to show the effect of anisotropy on such a situation, we take up the de Gennes layer model [13]. A spin (S) layer structure with J', J the (positive) intralayer and the (negative) interlayer exchange coupling, gives the exchange energy contribution:

$$E_{ex} = -Nz'J'S^2 + Nz|J|S^2 \cos\theta_0 \quad (1a)$$

In addition, Nx Zener carriers are supposed to move inside and in between layers with transfer integrals b' and b leading to a ferromagnetic coupling contribution E_D:

$$E_D = (-z'b' - zb\cos(\theta_0/2))Nx \quad (1b)$$

here the extended electron state phase sums are already reduced to the nearest neighbour coordination numbers z', z, i.e. one assumes a small number of polarized electrons (Nx) in the bottom of a conduction band ($k \approx 0$). Adding the Zeeman energy:

$$E_Z = -M_0 H\cos(\theta_0/2) \quad (1c)$$

and the first two terms of an uniaxial anisotropy energy:

$$E_{an} = K_1\sin^2\theta + K_2\sin^4\theta \quad (1d)$$

where the relation between the cant angle θ_0 and the deviation θ of a sublattice magnetization from the easy axis are shown in Fig. 6a. In that case $\theta_0/2 = 90 - \theta$ for $H \perp$ to the easy axis. Minimizing the total energy without anisotropy energy: $E_m = E_{ex} + E_D + E_Z$ in respect to θ_0, one always finds a canted structure at $T = 0$ with the cant angle θ_0 getting smaller when H increases. At elevated temperatures $T > 0$, and small enough carrier concentration x, antiferromagnetic long range order appears because of an entropy term, which arises from a competition of the thermal averages $\langle\cos\theta_0\rangle$ and $\langle\cos\theta_0/2\rangle$. The entropy difference one can write [33]:

$$S_m = S_0 - \alpha\langle\cos\theta_0/2\rangle + \ldots; \quad F = -TS_m + E_m \quad (1f)$$

If, for $T \to 0$ we can approximate the thermal averages by their angular functions, i.e. $\langle\cos\theta_0/2\rangle \to \cos\theta_0/2$, etc., from $\partial F/\partial\theta_0 = 0$ we obtain a second-order

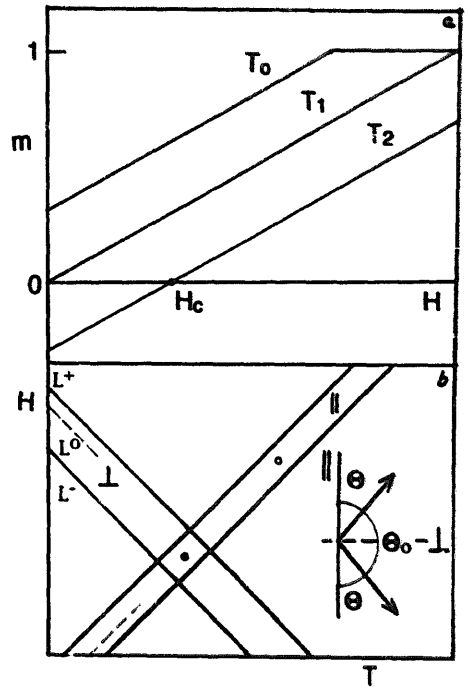

Fig. 6. (a) Reduced magnetization vs. field, $m(H)$, for a double-exchange/ superexchange model system showing second order temperature-and field-induced transitions without considering anisotropy. T_0,T_1: isotherms; H_c critical field for *afm*-canted transition at temperature T_2. (b) Lability and equilibrium lines L^+, L^-, L^0 lines for the canted and *afm* states in a H–T diagram considering anisotropy. Arrows, canted sublattices in respect to easy and hard axis; open (full) point, one(two) stable and one(two) metastable states (for more details see text).

field- or temperature or carrier localisation induced canted/*afm* transition, setting $m = 0$ or $\theta_0 = \pi$:

$$m = M/M_0 = \cos(\theta_0/2) = x/x_0 = T/T_0 + H/H_0 \quad (2)$$

where $\beta = 4\ Nz|J|S^2$; $x_0 = \beta/zNb$; $T_0 = \beta/\alpha$; $H_0 = \beta/M_0$, i.e. increasing the temperature lowers the $m(H)$ line to cross the H-axis at H_c, thus defining an *afm*-canted field- or temperature-induced transition. If $m(H)$ starts at the origin (0, 0), $H_c = 0$ and $T_1(x) = zbNx/\alpha$ describes the temperature-induced *afm*-canted transition line. If $H_c > 0$, $m(H)$ crosses the H-axis at H_c and $T_1(x) = zbNx/\alpha + M_0H_c/\alpha$) (Fig. 6a). The field-induced transitions close to T_1 (Fig. 2) could be of this type.

3.2. Field- and anisotropy-induced transitions

If we now allow for an anisotropy energy, we have to consider that the external field is either parallel or perpendicular to the easy axis (Fig. 6b). Then, for the free energies we have, substituting $y = \cos\theta_0/2$:

$$F = F_0(x,T) + A(x,H,T)\cdot y + B\cdot y^2 + C\cdot y^4; \quad \perp \text{ or } \| \quad (3)$$

with $F_o = -Nz'J'S^2 - z'b'Nx - Nz|J|S^2 - S_oT$; $B_\perp = 4Nz|J|S^2 + K_1$; $C_\perp = K_2$; $A_\perp = A\| - M_oH$; $A\| = -zbNx + \alpha T$; $B_\| = B_\perp + 4\chi_\| H^2 - K_1/2$; $C_\| = K_2/2 - 4\chi_\| H^2$

If the external field is parallel to the easy axis, the Zeeman energy is small as the field now acts mainly on the anti-ferromagnetic component; there remains, however, a small field-parallel susceptibility. In that case the Zeeman energy should be maximal at $\theta_o = \pi/2$ in a first approximation, i.e. $\sim \chi_\| H^2(1 - \cos^2\theta_o)$, as the magnetization component in the field direction is zero for both $\theta_o = 0, \pi$. This results in small field-dependent terms. Also, as the sublattices would become non-symmetric in respect to the $\|$ axis, the anisotropy energy is now expected to depend on two angles $\theta_{1,2}$; however, because of $\sin^2\theta$, it should be sufficient to consider the larger angle in this case.

If $K_2 = 0$, the *afm*-canted transitions could still be continuous, i.e. of second order, and metastable states would not occur. With $K_2 < 0$, the y^4 term would have a sign opposite to that of y^2 and metastable states, two each for $\perp$ and $\|$, are possible. This can be seen if one transforms Eq. (3) to the standard Landau expression for the free energy by interpreting the half-cant angle as an order parameter $\theta_o/2 = \eta$. For small $\theta_o/2$, $\cos(\theta_o/2) = 1 - \eta^2/2$, and neglecting terms with η^8 one can write:

$$F = F_o^* + a\eta^2 + b\eta^4 + c\eta^6 \quad \text{for each direction: } \perp, \| \tag{4}$$

with $a = B + 2C = A/2$, $F_o^* = F_o + A + B + C$; $b = c = B/4$, $c = C/2$; note, that if $K_2 < 0$, as usually found with similar ferromagnetic compounds [14–16,34], $c > 0$ and $b < 0$, i.e. we would obtain features of first order transitions, i.e. abrupt steps in the cant angle θ_o and the existence of two kinds of metastable and stable states. One metastable and one stable state can both exist at the same point in a metastable region of a, say, T–H phase diagram, depending on the thermodynamic paths chosen (Fig. 6b). As the stability lines L^+, L^- of such a metastable region are, in the Landau approximation, given by $a = 0$ (L^-) and $b^2 - 3ac = 0$ (L^+), and as $a_{\perp,\|}$ are known in our case, in principle we can calculate and draw the corresponding lines into a H–T diagram. For that we note that $a_\perp(H,T) = 0$ gives a nearly linear relation $(T - T_o) \sim (H - H_o)$, while $a_\|(H,T) = 0$ gives a small quadratic dependence $(T - T_o) \sim (H - H_o)^2$; as b^2 is only weakly dependent on H, the upper lability lines L^+ are almost parallel to L^-. The metastable regions might overlap or stay separate. The simplest case of the first kind would be two pairs of linear lability lines $H(T)$ intersecting as drawn in Fig. 6b. This allows to discuss more than one metastable state, such as found experimentally in Fig. 5. While a point in an isolated hysteretic region allows for two magnetic states, a point in the double occupied region in principle allows for four magnetic states. Inside an isolated hysteretic region, the location of the equilibrium line L^o (defined by $b^2 - 4ac = 0$) determines which state is metastable and which is stable at a given point. The situation is not so clear in case of a double hysteretic region. However, more than two stable and metastable states and transitions between them have been considered [35].

For $x = 0.17$ at $T = 10$ K, we have helical to canted transitions with increasing temperature (at T_K), while the calculation relates to canted/*afm* transitions with increasing temperature. The lower transition has been attributed to carrier localisation effects [12,17,18] However, metastable states equivalent to those described above can be assumed to exist also here when the anisotropy is included.

3.3. Clamped metastable state in $MnAs_{0.97}P_{0.03}$

The first order magnetic transition of $MnAs_{0.97}P_{0.03}$ at T_c has been recognized as a coupled lattice and magnetic transition [5,19] and as the variation with x has been found equivalent, to a large extent, to the application of pressure to MnAs, it is tempting to assign the irreversible change at T_{fm} at first heating to a release of some as grown internal strains of the single crystal. However, at low temperatures strains cannot be released by the thermal activation of lattice defects. Possibly, the transition from a spin-compensated state [10,21] to anti-ferromagnetic long range order at T_N is connected with a volume change which triggers the strain release. A significant volume change is indeed observed at T_c, i.e. with *afm* ordering (see Fig. 1). Such a strain release would be equivalent to a partial pressure release in a MnAs sample under pressure as shown in Fig. 7. Then, the recurrence of ferromagnetism at T_{fm} can happen if the lability lines are curved. This is found both experimentally and theoretically [20–25].

In particular, the different states of a sample on the first heating and cooling cycle, assuming a pressure, x and strain equivalence, are given by the path 1–7 in Fig. 7. At high temperatures, the sample is paramagnetic, then spin-glass-like and finally moves into the metastable region; after passing T_N(2), the internal strain gets relieved, as indicated by lines 2–3–4 or 2–4. When the temperature is subsequently increased, one first passes the inner lability line (L^-) from below (5), i.e. ferromagnetism should appear, as is observed at T_{fm}. With a further increase in the temperature, *fm* gets lost (6), but only at T_{ch}, as one approaches the outer lability line L^+ from the inside.

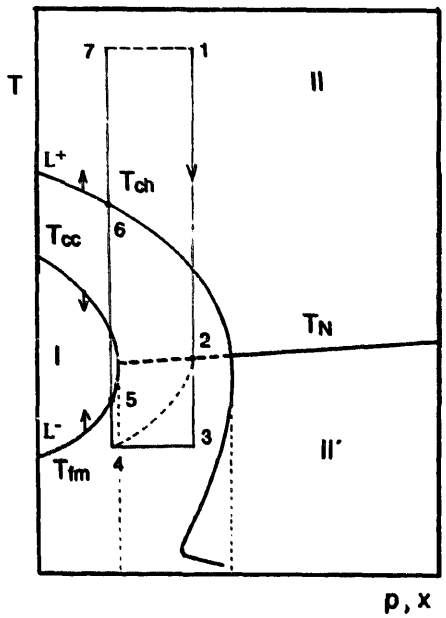

Fig. 7. Schematic P–T and x–T phase diagram for MnAs and $MnAs_{1-x}P_x$: 1–7, thermodynamic path chosen to explain Fig. 1; curved lines, lability lines of first order *fm*–*sg* transition for P–T diagram; straight line, *afm*–*sg* transition $T_N(x)$ or $T_N(p)$; dashed vertical lines, lower part of lability lines in case of x–T diagram (for more details see text).

With the next cooling, ferromagnetism reappears at T_{cc}, but is not lost when one crosses the lower section of the L⁻-line, as one approaches that line from the inside. After the crossing, the sample is, however, in a metastable ferromagnetic state; that is sometimes detected via structure in other physical properties [26,27]. At the 'metastable *fm*' to *fm* transition on heating, the magnetisation practically does not change. The changes in resistivity support this interpretation. The resistivity $\rho(T)$ is supposed to be mainly determined by spin disorder scattering [28–32] and therefore should look like an inverted magnetization curve [29], which is observed. The resistivity along the (100) -direction (Fig. 1b) shows only a very small structure at T_{fm}, consistent with the idea that *afm* long-range order is replaced by *fm* long-range order, while the resistivity changes at the spin order–disorder transitions T_c (20%) and T_{ch} (factor of 3) are larger.

Acknowledgements

The authors thank the Deutsche Forschungsgemeinschaft for continuous support, R. Burckart for the dilatation measurements and P. Mandal and E.A. Zavadskii for helpful discussions.

References

[1] A. Roger, R. Fruchardt, Mater. Res. Bull. 3 (1968) 253.
[2] K. Bärner, Phys. Status Solidi A 8 (1971) 119.
[3] Ch. Kleeberg, Diploma Thesis, Göttingen, 1993
[4] C. Guillaud, J. Phys. Radium 12 (1951) 223.
[5] C.P. Bean, D.S. Rodbell, Phys. Rev. 126 (1962) 104.
[6] H. Berg, K. Bärner, W. Schröter, Phil. Mag. 31 (1975) 1049.
[7] H. Fjellvag, A.F. Andresen, K. Bärner, J. Magn. Magn. Mater. 46 (1984) 29.
[8] H.W. Helberg, B. Wartenberg, Z. Angew. Phys. 20 (1966) 505.
[9] G.W. Schaumburg, Thesis, Göttingen, 1992
[10] G.A. Govor, A.K. Vecher, Ch. Kleeberg, J.W. Schünemann, V. Dankelmann, K. Bärner, Phys. Status Solidi A 138 (1993) 307.
[11] K. Bärner, Phys. Status Solidi B 88 (1978) 13.
[12] H. Berg, K. Bärner, J. Magn. Magn. Mater. 4 (1977) 69.
[13] P.G. de Gennes, Phys. Rev. 118 (1960) 141.
[14] W.P. Mason, Phys. Rev. 96 (1954) 302.
[15] H.J. Kohnke, Ch. Kleeberg, V. Dankelmann, K. Bärner, J.W. Schünemann, J. Alloys Comp. 239 (1996) 150.
[16] H.J. Kohnke, V. Dankelmann, Ch. Kleeberg, J.W. Schünemann, K. Bärner, A. Vetcher, G.A. Govor, Phys. Status Solidi B 191 (1995) 511.
[17] G. Bödecker, K. Bärner, K. Funke, Phys. Status Solidi B 98 (1980) 571.
[18] K. Bärner, E. Gmelin, Phys. Status Solidi B 132 (1985) 431.
[19] A. Erle, K. Bärner, J. Magn. Magn. Mat. 74 (1988) 225.
[20] M. Menyuk, J.A. Kafalas, K. Dwight, J.B. Goodenough, Phys. Rev. 177 (1969) 942.
[21] J.W. Schünemann, A. Lange, G.A. Govor, K. Bärner, E. Gmelin, J. Alloys Comp. 178 (1992) 237.
[22] A. Zieba, H. Fjellvag, A. Kjekshus, J. Phys. Chem. Solids 46 (1985) 275.
[23] E.A. Zavadskii, B.Ya. Sukharevskii, Fiz. Nizk. Temp. (Low Temp. Physics) 21 (1995) 856.
[24] K. Bärner, E.A. Zavadskii, Ber. der Bunsenges. Phys. Chem. 100 (1996) 155.
[25] E.A. Zavadskii, Private Communication
[26] B. Kirchschlager, H. Berg, K. Bärner, Phys. Lett. 82A (1981) 46.
[27] J. Ihlemann, H.J. Krokoszinski, E. Gmelin, K. Bärner, Phys. Stat. Sol. 87 (1985) 279.
[28] K. Bärner, Phys. Status Solidi B 84 (1977) 385.
[29] C.W. Searle, S.T. Wang, Can. J. Physics 48 (1970) 2023.
[30] K. Bärner, U. Neitzel, Phys. Lett. 91A (1982) 361.
[31] G.A. Govor, K. Bärner, J.W. Schünemann, Phys. Status Solidi A 113 (1989) 403.
[32] V. Dankelmann, H.J. Konnke, J.W. Schünemann, K. Bärner, S. Buzhinsky, I.V. Medvedeva, J. Alloys Comp. 209 (1994) 305.
[33] K. Bärner, L. Haupt, R.v. Helmolt, Phys. Status Solidi B 187 (1995) K61.
[34] Ch. Kleeberg, E. Kraus, K. Bärner, T. Gron, U. Sondermann, Radiation Effects and Defects in Solids, Gordon and Breach Science, 1997, in print.
[35] K. Bärner, E.A. Zavadskii, Ferroelectr. Lett., G.W. Taylor (Ed.), V23 No. 1/2, 1997, in print.